Fragmentation cross sections of ^{16}O, ^{24}Mg, and ^{32}S projectiles at 3.65 GeV/nucleon

D. Sampsonidis, E. Papanastassiou, and M. Zamani
Physics Department, University of Thessaloniki, 540 06 Thessaloniki, Greece

M. Debeauvais and J. C. Adloff
Centre de Recherches Nucleaires, F-67037 Strasbourg Cedex 2, France

B. A. Kulakov, M. I. Krivopustov, and V. S. Butsev
Joint Institute for Nuclear Research, 141980 Dubna, Russia
(Received 28 September 1994)

We have investigated the fragmentation of 3.65 GeV/nucleon ^{16}O, ^{24}Mg, and ^{32}S projectiles on C, Al, Cu, Ag, and Pb targets using solid state nuclear track detectors. Track counting was performed by an automatic measuring system. Total charge changing and the partial cross sections for the production of fragments with charges $9 \leq Z \leq 15$ for ^{32}S projectiles and of charge $6 \leq Z \leq 11$ for ^{24}Mg were determined. Comparison with theoretical models and other experimental data is made.

PACS number(s): 25.75.+r, 25.70.Mn

I. INTRODUCTION

Experimental results on total charge changing and partial cross sections give information on peripheral reactions at relativistic energies. They also have application to astrophysical problems, especially understanding the cosmic ray propagation. Fragment production cross sections can provide the basis for theoretical studies on the interaction process of high-energy collisions. Since the charged fragments originating from projectile breakup maintain most of the projectile longitudinal velocity, they can be identified using the relation between nuclear charge Z and dE/dX. Charge identification in solid state nuclear track detectors (SSNTD) depends on this relationship. The detection principle of SSNTD is based on the fact that when an ionizing particle passes through an insulating solid, it creates a chemically reactive radiation-damaged region along its trajectory [1]. By an appropriate chemical treatment, the damaged regions of the detector material are etched with a velocity ν_T (track etch velocity) and the undamaged material with a constant velocity ν_B (bulk etch velocity), where $\nu_T > \nu_B$. As a result, an etched cone (nuclear track) is formed which is visible under a microscope. What we see in the present case is the intersection of the etched cone with the detector surface. In most cases, this is a dark ellipse or circle on a brighter background.

The track etch velocity ν_T is a function of the restricted energy loss (REL), defined as that part of the energy loss due to ionizations where δ electrons with an energy below a value w_0 are generated. In the CR39 used, w_0 has been determined to be 200 eV [2].

Somogyi and Szalay [3] have derived the relation between ν_T, ν_B, and the radius R of a circular track:

$$\nu_T = \nu_B \frac{(\nu_B t)^2 + R^2}{(\nu_B t)^2 - R^2} , \qquad (1)$$

where t is the etching time.

Since $\nu_T = f_1(\mathrm{REL})$ and $\mathrm{REL} = f_2(Z,E)$, $\nu_T = f_3(Z,E)$ or equivalently $R = f(Z,E)$ because the relation between R and ν_T is known. For energies above 800 MeV/nucleon, the REL remains approximately constant. Therefore R can be considered to be a function of only Z [4].

The experimental setup for measuring the projectile fragmentation cross sections is shown in Fig. 1. A stack of three CR39 foils is placed upstream of the target in order to register the incoming beam particles. Another stack of three CR39 foils is placed downstream to identify the outgoing beam particles and projectile fragments.

The stacks were exposed perpendicularly to the beam axis at the Dubna LHE synchrophasotron. The beam of ^{32}S, contaiminated with about 40% ^{16}O at 3.65 GeV/nucleon, had a total intensity of 4×10^3 ions/cm^2. The ^{24}Mg beam had the same energy per nucleon and an intensity of 1×10^4 ions/cm^2. The CR39 was etched afterwards in $6N$ NaOH at 70 °C for about 50 h.

II. IMAGE ANALYSIS SYSTEM

For scanning the detector surfaces and measuring the track radii, an automatic measuring system based on image analysis techniques was used [5]. The principal com-

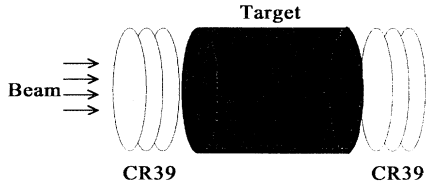

FIG. 1. Experimental setup.

ponents of the system are a PC computer with a frame grabber, an image display monitor, a microscope with a motorized stage, and a video camera. The software for the image analysis and track recognition has been specifically developed to fulfill the requirements of automatic measurements.

A detector foil is scanned by moving the motorized microscope stage under computer control. The image of the microscope is viewed by the video camera and digitized by the frame grabber to a 512 × 512 pixel digital image. Nuclear tracks appear as dark areas recognized by the software. For each track the parameters determined are the radius, coordinates of the center, and the brightness in the center of the track.

III. EXPERIMENTAL RESULTS

Tracks were measured upstream and downstream of C, Al, Cu, Ag, and Pb targets using the image analysis system. As an example of the as-measured data, we present in Fig. 2 the distribution of radii obtained downstream for ^{24}Mg on a Pb target. The large peak is due to beam particles which came out of the target without undergoing a nuclear reaction. No other peaks corresponding to intermediate fragments produced by projectile fragmentation are easily distinguished. The measurements were further processed to: (i) reject tracks due to detector background, and (ii) correct projected track area due to inhomogeneous stage illumination.

The data of Fig. 2 are shown in Fig. 3 after this processing. A peak for each fragment charge from $Z = 6$ to $Z = 12$ now appears.

A numerical fitting method using successive minimizations have been used to fit the radius distributions with the appropriate number of Gaussian peaks, each corresponding to a fragment charge. The parameters which have to be estimated are the peak position, the FWHM, and the height. These parameters permit the calculation of each peak integral. The quality of fit was estimated by

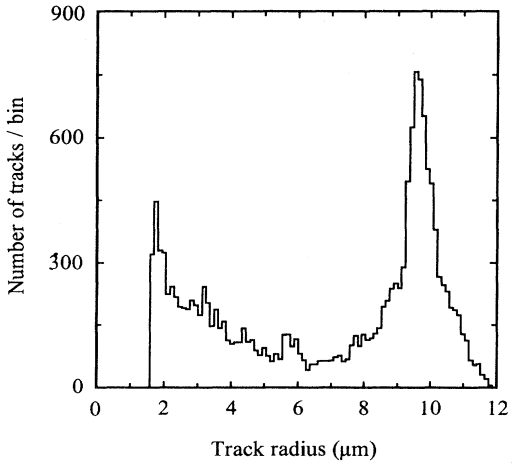

FIG. 2. Track radius distribution of ^{24}Mg fragmentation on Pb target (downstream).

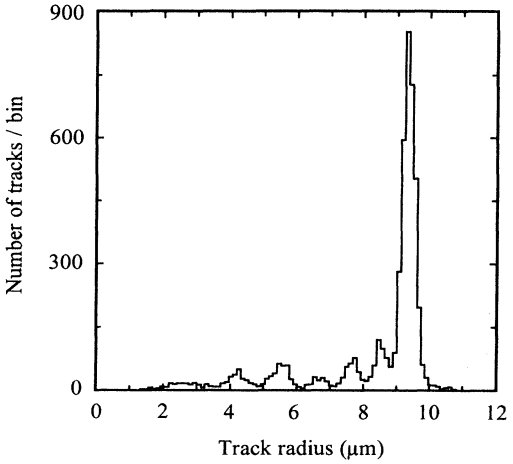

FIG. 3. Track radius distribution of ^{24}Mg fragmentation on Pb target (downstream) after corrections.

the reduced χ^2. Its value was between 0.1 and 1.0 for the different spectra. A linear relation between track radius and the peak position was found, which is equivalent to a linear correlation of track radius with fragment charge Z. From the standard deviation of each peak and this linear relationship, the charge resolution in these experiments was found to be of the order of 0.25 elementary charge.

IV. TOTAL AND PARTIAL CROSS SECTIONS

From the number of tracks measured for each charge Z upstream and downstream of the target, the total and partial cross sections were calculated using the formula [6]:

$$N_i(x) = N_i(0)e^{-x\sigma_i} + \sum_{j=1}^{i-1} k_{ij}(e^{-x\sigma_j} - e^{-x\sigma_i}) \ , \qquad (2)$$

$$k_{ij} = \frac{1}{\sigma_i - \sigma_j}\left\{\sigma_{ij}N_j(0) - \sum_{n=j+1}^{i-1}\sigma_{in}k_{nj} + \sum_{n=1}^{j-1}\sigma_{ij}k_{jn}\right\} ,$$

where x is the surface density of the target, $x = N_A\rho t/A$, N_A Avogadro's number, ρ target density, A_T target atomic number, t depth in the target, $N_i(0)$ number of tracks of charge Z_i at $x = 0$, where for the ^{32}S expsoure $Z_1 = 16$ and $Z_{10} = 7$, and for ^{24}Mg exposure $Z_1 = 12$ and $Z_7 = 6$, $N_i(x)$ same as $N_i(0)$ at arbitrary x, σ_i total charge changing cross section of nucleus with charge Z_i in the target, σ_{ij} partial cross section of the production of a projectile fragment of charge Z_i in a collision of a projectilelike of charge Z_j on the target.

Concerning the choice of target thickness, a compromise was necessarily made between two conflicting requirements: The target should be thin enough to minimize multiple interactions and beam energy loss, and thick enough to produce a high interaction rate. The thickness of the targets used in this experiment was rather large, between 20% and 35% of the ^{32}S interac-

tion mean free path. The use of Eq. (2) in calculating the partial cross sections takes into account multiple interactions in the thick target.

The presence of ^{16}O in the ^{32}S beam in fact permitted obtaining results for both projectiles. In Fig. 4 the total charge changing cross sections are presented as a function of target mass A_T. For the $Z = 8$ coming from ^{32}S a correction had to be made for the ^{16}O beam particles in the $Z = 8$ peak. A smooth extrapolation of the $\Delta Z = 7, 6, 5$ results permits estimation of the number of $Z = 8$ fragments coming from ^{32}S, and thus by difference the attenuation (total charge changing cross section) of the ^{16}O beam in the targets. The $Z = 8$ particles from ^{32}S form about 0.1% of the total $Z = 8$ peak, corresponding to a 0.7% reduction in the total charge changing cross section of ^{16}O which is negligible compared to the experimental uncertainties. Errors on total charge changing cross sections as well as on partial cross sections were calculated taking into account the weighting factors based on the experimental error on track counting [7].

The total charge changing cross sections derived using the Eq. (2) were compared with theoretical values according to several models. One of them is the geometrical model of Bradt and Peters [8]:

$$\sigma = \pi r_0^2 (A_P^{1/3} + A_T^{1/3} - b)^2 , \quad (3)$$

where A_P, A_T are the projectile and target mass number, respectively, r_0 the nuclear radius constant ($r_i = r_0 A_i^{1/3}$), and b the overlap parameter, which is assumed to be constant. The values taken for r_0 and b were 1.20 fm and 1.32, respectively.

The above relation was modified by Barshay *et al.* [9] based on the soft-sphere model [10]. In the modified expression for the total charge changing cross section, the parameter b is not constant and is expressed as

$$b = b_0 (A_P^{-1/3} + A_T^{-1/3}) \quad (4)$$

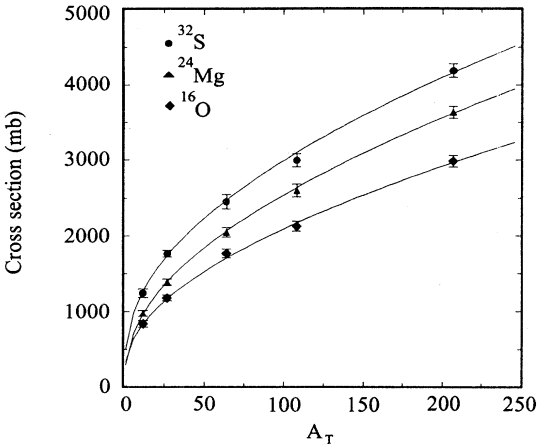

FIG. 4. Total charge changing cross sections as a function of target mass A_T for ^{32}S, ^{24}Mg, and ^{16}O.

with $b_0 = 0.72$. b_0 is the curvature correction parameter and accounts for the nuclear surface deformation during the collision.

The best agreement with our results, for the three different projectiles, was obtained by using Eq. (3) with the overlap parameter as expressed in Eq. (4). Keeping in mind that the parameter r_0 should be constant and independent of A_P and A_T, the data were fitted using Eq. (3) with r_0 set at 1.35 fm, which is a commonly used value in the literature [7,11]. The parameter b and the reduced χ^2 were calculated to be

^{32}S	$b = 0.51 \pm 0.03$	$\chi^2 = 1.51$,
^{24}Mg	$b = 0.82 \pm 0.04$	$\chi^2 = 1.60$,
^{16}O	$b = 0.94 \pm 0.04$	$\chi^2 = 1.10$.

The results show a dependence of the overlap param-

TABLE I. Total charge changing cross sections for ^{16}O, ^{24}Mg, and ^{32}S at 3.65 GeV/nucleon determined in the present experiment and other experimental data in the same range of projectile energies. The data from Webber *et al.* [15] are for 1.56 GeV/nucleon for ^{16}O, 1.45 GeV/nucleon for ^{24}Mg, and 1.14 GeV/nucleon for ^{32}S. The data from Brechtmann and Heinrich [18] correspond to 1.2 GeV/nucleon for Al and Cu targets and 0.7 GeV/nucleon for C and Ag targets. The data from Lindstrom *et al.* [19] correspond to 2.1 GeV/nucleon.

Beam	Target	σ_{tot} (mb)			
		This work	Ref. [15]	Ref. [18]	Ref. [19]
	C	1244 ± 55	1269 ± 13	1250 ± 21	
	Al	1761 ± 43		1771 ± 26	
^{32}S	Cu	2451 ± 94		2428 ± 61	
	Ag	2993 ± 87		3034 ± 83	
	Pb	4189 ± 93			
	C	1009 ± 36	1133 ± 11		
	Al	1386 ± 41			
^{24}Mg	Cu	2048 ± 61			
	Ag	2446 ± 85			
	Pb	3439 ± 81			
	C	843 ± 45	851 ± 9		1022 ± 25
	Al	1169 ± 38			
^{16}O	Cu	1765 ± 59			1950 ± 41
	Ag	2125 ± 65			
	Pb	2985 ± 75			3270 ± 82

eter on the small mass involved in the reaction in agreement with the results of Heckman *et al.* [12]. In our experiments the smaller mass was that of the projectile in most cases.

Expressions proposed by Hagen [13], Binns *et al.* [14], and Webber *et al.* [15] also fit our results well. The parameters estimated in each case are quite different from those given in the references even though the results show acceptable χ^2 values. Keeping in mind that there is no significant energy dependence of total charge changing cross section over the range from a few hundred MeV/nucleon to a few GeV/nucleon [11], we conclude that all these relations are acceptable with different parameters. In most cases, the data reported refer to systems lighter than ours.

When the geometrical model is used to fit our data, a correction for electromagnetic dissociation effects should be applied, especially for the heavier targets. Its contribution to the total charge changing cross sections was calculated using the Weizsacker-Williams method [16] and found to be about 10% for the Pb target and 6% for the Ag target. For the lighter targets this contribution was of the same order of magnitude as the experimental errors [17] and no correction was applied.

Table I presents the total charge changing cross sections for ^{16}O, ^{24}Mg, and ^{32}S determined in the present experiments and experimental data of others [15,18,19].

An iterative program has been used to calculate the partial cross sections for projectile fragmentation. This program assumes that for a given charge loss ΔZ, the ratio of the partial cross sections to the total charge changing cross sections for a given ΔZ is constant for all Z in this range of Z [14]. For the total charge changing cross sections, the program used the Bradt-Peters formula with parameters calculated by fitting the data of the present experiment.

In Figs. 5 and 6, partial cross sections are shown for ^{24}Mg and ^{32}S projectiles, respectively. Partial cross sections for fragment production with charge $6 \leq Z \leq 11$ from ^{24}Mg and $9 \leq Z \leq 15$ from ^{32}S fragmentation were calculated using Eq. (2). The ^{16}O data are not presented, because of the limited number of experimental points, $Z = 6$ being our detection limit.

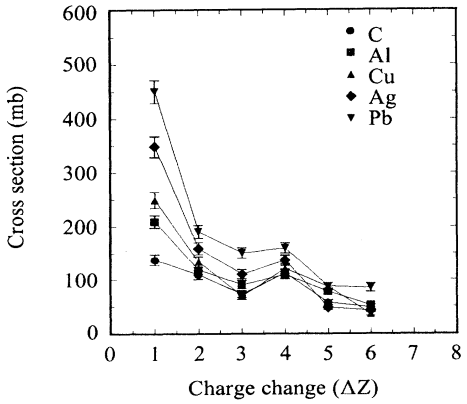

FIG. 5. Partial cross sections for ^{24}Mg, at 3.65 GeV/nucleon on C, Al, Cu, Ag, and Pb targets as a function of charge change ΔZ.

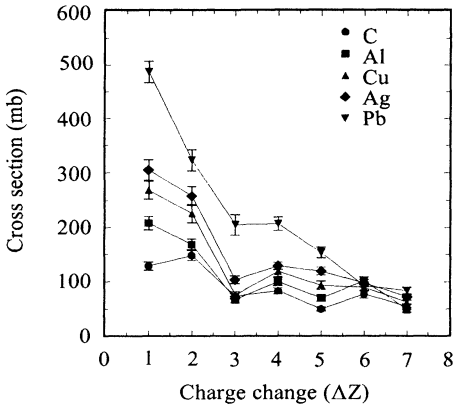

FIG. 6. Partial cross sections for ^{32}S at 3.65 GeV/nucleon on C, Al, Cu, Ag, and Pb targets as a function of charge change ΔZ.

A regular decrease of $\sigma(\Delta Z)$ with ΔZ is observed. The cross sections $\sigma(\Delta Z)$ depend on the target. Heavier targets give larger partial cross sections with increasing difference at smaller ΔZ (Figs. 5, 6). Similar results have been found, for example, for ^{56}Fe projectiles on about the same set of targets at 1.88 GeV/nucleon [11].

Comparison of our results with the data of Webber *et al.* [20] for ^{32}S and ^{24}Mg projectiles on C targets at respective beam energies of 1.15 and 1.45 GeV/nucleon shows agreement within 7.5%. Similar experimental methods for ^{32}S on Al and Cu at 1.2 GeV/nucleon and for ^{32}S on C and Ag at 0.7 GeV/nucleon [18] show agreement within 11%.

The cumulative fraction of the partial cross sections $\sigma(\Delta Z)$ as a function of the charge change ΔZ is plotted in Fig. 7 for ^{24}Mg and ^{32}S projectiles. Partial cross sections were summed to Z of about half of the projectile charge.

In the case of the ^{24}Mg beam, the figure shows that the percentage of total fragmentation from the Cu, Ag, and

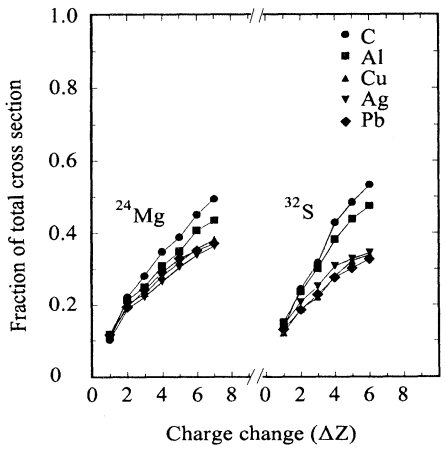

FIG. 7. The incremental fraction of the total charge changing cross sections as a function of the cumulative charge change ΔZ.

Pb targets is almost constant (about 30%), whereas the corresponding values for the lighter targets are considerably higher, namely 45% and 55% for Al and C targets, respectively. This behavior, which is also observed in other experiments [14,20], shows that the lighter targets have a greater probability for fragment production and especially for small Z fragments. The same behavior is also observed with ^{32}S projectiles. The percentage fragmentation reached by Cu, Ag, and Pb targets is about 35% of the total cross section, whereas for C and Al targets these values are about 50% and 45%, respectively.

V. CONCLUSIONS

We have used SSNTD to measure total and partial charge changing cross sections for ^{16}O, ^{24}Mg, and ^{32}S on C, Al, Cu, Ag, and Pb at 3.65 GeV/nucleon.

The total charge changing cross sections can be well described by a geometrical model with an overlap parameter depending on both target and projectile masses. The smaller mass involved in the collision contributes the greater part of the overlap parameter.

The partial cross sections are target dependent. Fragment production from the projectiles is higher for small ΔZ and decreases with increasing ΔZ. Fragment production with small ΔZ is higher for heavier targets. Partial cross sections account for up to half of the total charge changing cross section. For C and Al targets this fraction is inversely proportional to the target mass. For Cu, Ag, and Pb the fraction of the total charge changing cross section appears to be almost target independent.

ACKNOWLEDGMENTS

We are grateful to the staff of the Synchrophasotron at the Joint Institute for Nuclear Research (Dubna) for providing the heavy-ion beams. We wish to express our appreciation to A. Pape for useful discussions.

[1] R. L. Fleischer, P. B. Price, and R. M. Walker, *Nuclear Tracks in Solids* (University of California Press, Berkeley, 1975).
[2] D. L. Henshaw, N. Griffiths, A. L. Landen, and E. V. Benton, Nucl. Instrum. Methods **180**, 65 (1981).
[3] G. Somogyi and S. A. Szalay, Nucl. Instrum. Methods **109**, 211 (1973).
[4] J. Dreute, W. Heinrich, G. Rush, and B. Wiegel, Phys. Rev. C **44**, 1057 (1991).
[5] D. Sampsonidis and M. Zamani, Microprocessing and Microprogramming **34**, 153 (1992).
[6] C. Brechtmann and W. Heinrich, Nucl. Instrum. Methods. **B29**, 675 (1988).
[7] P. B. Price and Y. D. He, Phys. Rev. C **43**, 835 (1991).
[8] H. C. Bradt and B. Peters, Phys. Rev. **77**, 54 (1950).
[9] S. Barshay, C. B. Dover, and J. P. Vary, Phys. Rev. **11**, 360 (1975).
[10] P. J. Karol, Phys. Rev. C **11**, 1203 (1975).
[11] G. D. Westfall, L. W. Wilson, P. J. Lindstrom, H. J. Crawford, D. E. Crawford, D. E. Greiner, and H. H. Heckman, Phys. Rev. C **19**, 1309 (1979).
[12] H. H. Heckman, D. E. Greiner, P. J. Lindstrom, and H. Shwe, Phys. Rev. **17**, 1735 (1978).
[13] F. Hagen Ph.D. thesis, University of Maryland, 1976.
[14] W. R. Binns, T. L. Garrard, M. H. Israel, M. P. Kertzmann, J. Klarmann, E. C. Stone, and C. J. Waddington, Phys. Rev. C **36**, 1870 (1987).
[15] W. R. Webber, J. C. Kish, and D. A. Schrier, Phys. Rev. **41**, 520 (1990).
[16] J. D. Jackson, *Classical Electrodynamics*, 2nd ed. (Wiley, New York, 1975).
[17] D. Sampsonidis, Ph.D. thesis, University of Thessaloniki, 1994.
[18] C. Brechtmann and W. Heinrich, Z. Phys. A **331**, 463 (1988).
[19] P. J. Lindstrom, D. E. Greiner, and H. H. Heckman, Bull. Am. Phys. Soc. **17**, 54 (1970).
[20] W. R. Webber, J. C. Kish, and D. A. Schrier, Phys. Rev. **41**, 533 (1990).